JACS
JOURNAL OF THE AMERICAN CHEMICAL SOCIETY

Article

pubs.acs.org/JACS

Polymorph Selectivity of Superconducting $CuSe_2$ Through Kinetic Control of Solid-State Metathesis

Andrew J. Martinolich, Joshua A. Kurzman, and James R. Neilson*

Department of Chemistry, Colorado State University, Fort Collins, Colorado 80523-1872, United States

Supporting Information

ABSTRACT: Rational preparation of materials by design is a major goal of inorganic, solid-state, and materials chemists alike. Oftentimes, the use of nonmetallurgical reactions (e.g., chalcogenide fluxes, hydrothermal syntheses, and in this case solid-state metathesis) alters the thermodynamic driving force of the reaction and allows new, refractory, or otherwise energetically unfavorable materials to form under softer conditions. Taking this a step further, alteration of a metathesis reaction pathway can result in either the formation of the equilibrium marcasite polymorph (by stringent exclusion of air) or the kinetically controlled formation of the high-pressure pyrite polymorph of $CuSe_2$ (by exposure to air). From analysis of the reaction coordinate with *in situ* synchrotron X-ray diffraction and pair distribution function analysis as well as differential scanning calorimetry, it is clear that the air-exposed reaction proceeds via slight, endothermic rearrangements of crystalline intermediates to form pyrite, which is attributed to partial solvation of the reaction from atmospheric humidity. In contrast, the air-free reaction proceeds via a significant exothermic process to form marcasite. Decoupling the formation of NaCl from the formation of $CuSe_2$ enables kinetic control to be exercised over the resulting polymorph of these superconducting metal dichalcogenides.

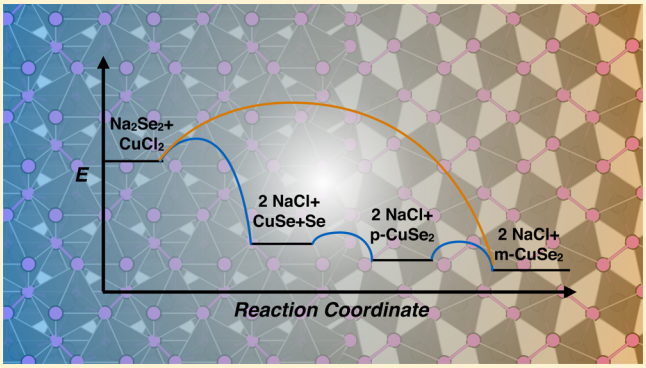

INTRODUCTION

In preparative solid-state chemistry, different polymorphs are often selected by changing extrinsic parameters to favor distinct atomistic configurations with the lowest thermodynamic free energy. While many extrinsic factors influence polymorph thermodynamic stability, such as pressure (graphite vs diamond), temperature (ZnS),[1] and specific surface area (TiO_2),[2] such polymorphs can be kinetically stable (i.e., metastable) at ambient conditions. However, kinetic control, in this case, the ability to prevent a system from reaching the thermodynamic equilibrium product, can be exercised through alteration of the pathway to product formation. This is largely unexplored in the formation of bulk, solid-state materials.

Transition-metal chalcogenides of the pyrite structural family give rise to myriad functional electronic properties, including superconductivity (cf., CuS_2, $CuSe_2$, $IrSe_2$);[3,4] however, many of these crystals can be produced only at high pressure. $CuSe_2$ exists in two known polymorphs: marcasite $CuSe_2$ and the high-pressure phase, pyrite $CuSe_2$, which is metastable under ambient conditions (Figure 1).[5] The superconducting transition temperature is strongly influenced by the structure: T_c = 2.4 and 0.7 K for pyrite and marcasite, respectively.[3,6]

The preparation of metastable materials (without the use of other extrinsic thermodynamic parameters, such as pressure) often involves chimie douce reactions,[7−11] where a difference in relative mobilities of ions in the lattice permits topochemical transformations into metastable polymorphs, as first exemplified by the oxidative deintercalation of $LiVS_2$ to yield a new

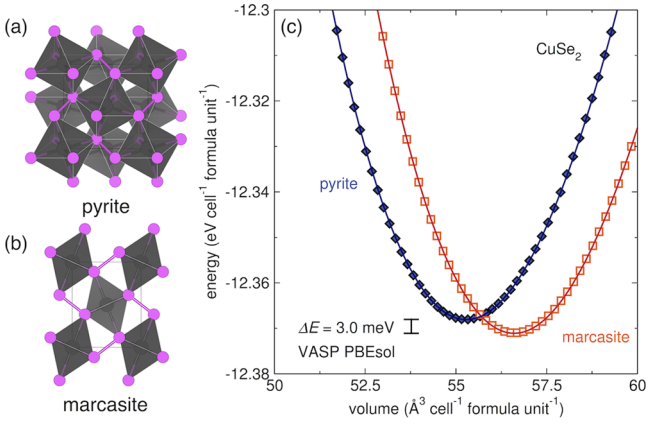

Figure 1. Atomistic representations of (a) pyrite and (b) marcasite polymorphs of $CuSe_2$. (c) The total energy from DFT calculations (VASP, PBEsol) illustrate that marcasite is more stable by a small margin (~3.0 meV); approximately 1.2 GPa of external pressure stabilizes pyrite $CuSe_2$. Symbols result from individual DFT calculations; lines are fits to the Birch−Murnaghan equation-of-state.[15]

Received: December 9, 2014
Published: March 6, 2015

DOI: 10.1021/ja512520z
J. Am. Chem. Soc. 2015, 137, 3827−3833

polymorph of VS_2.[12] However, examples in which metastable polymorphs can be produced through kinetic control without such topochemical relations are not widely understood. High-temperature solvents, such as the reactive alkali chalcogenide fluxes, can be used to produce compounds that are metastable under ambient conditions;[13] however, an understanding of the kinetic pathways or thermodynamic conditions that control their formation is limited.[14]

In this work, kinetic control over the formation of distinct polymorphs of the superconductor $CuSe_2$ is demonstrated by altering the pathway through which a solid-state metathesis reaction occurs. Preparation of the pyrite modification of $CuSe_2$ (p-$CuSe_2$) in 100% yield typically requires application of pressure in excess of 1 GPa,[3] in agreement with the reported equilibrium phase diagram[16] and density functional theory (DFT) calculations (Figure 1c). In the metathesis reaction (i.e., double-displacement) between $CuCl_2$ and Na_2Se_2, marcasite $CuSe_2$ and 2 NaCl are produced when performed under strictly anhydrous conditions. However, partial solvation of the reaction mixture by exposure to humid air before heating (and not exposure to dry O_2) enables the formation of bulk pyrite $CuSe_2$. By following the air-exposed reaction *in situ*, we observe that the solid-state metathesis occurs through endothermic and displacive transitions involving crystalline intermediates rather than through an exothermic and reconstructive transition. Partial solvation of the reaction mixture greatly reduces the initial activation barrier and allows the reaction to proceed under kinetic control, where the rate-limiting step appears to be diffusion of elemental selenium into the reaction intermediate CuSe, which forms upon air exposure.

MATERIALS AND METHODS

Na_2Se_2 was synthesized from the elements with a 2% excess of Na to account for surface oxidation in a sealed tube at 400 °C. The reactants were separately contained in different alumina crucibles to prevent a violent thermite reaction; after 12 h of reaction all product was found in the crucible originally containing the sodium. Purity of the Na_2Se_2 was confirmed through PXRD using a Bruker APEX II single crystal diffractometer (Mo$K\alpha$ radiation, λ = 0.7107 Å) with powder in a sealed quartz capillary; the two-dimensional (2D) data were radially integrated for analysis. Otherwise, laboratory PXRD measurements were collected on a Scintag A2 diffractometer with CuK_α radiation.

To isolate pure pyrite $CuSe_2$, stoichiometric amounts of Na_2Se_2 and anhydrous $CuCl_2$ were weighed in an argon-filled glovebox and ground to an homogeneous powder. Upon removal from the glovebox, the powder was further ground until a color change from deep brown to black was evident. The black powder was then pelleted and sealed in an evacuated fused silica ampule and heated to 100 °C at a rate of 1 °C min^{-1} and held constant for 24 h. Control reactions were held at 100 °C for 72 and 1008 h. The products were then washed several times with anhydrous methanol to remove the NaCl and dried under vacuum.

To form marcasite $CuSe_2$, stoichiometric amounts of Na_2Se_2 and anhydrous $CuCl_2$ were weighed in an argon-filled glovebox and ground to a homogeneous powder and pelleted. The pellet was then sealed in an evacuated quartz ampule without exposure to the atmosphere and heated to 300 °C at a rate of 1 °C min^{-1} and held constant for 24 h.

CuSe was formed from the elements at 300 °C in a sealed tube for 24 h. The product was then ground together with selenium shot until homogeneous, pelleted, and reacted in an evacuated quartz ampule to form $CuSe_2$ at 100 °C for the specified times. Additionally, marcasite $CuSe_2$ (formed by metathesis) was ground homogeneously with 2 equiv of NaCl, pelleted, sealed in a quartz ampule under vacuum, and reacted at 100 °C for the specified times.

In situ X-ray diffraction experiments were executed using beamline 17-BM-B (λ = 0.75009 Å) at the Advanced Photon Source at Argonne National Laboratory. The reaction mixture was ground in air and packed into a 0.4 mm diameter capillary and sealed under vacuum. To heat the reaction mixture, a resistive heater and thermocouple were used as previously described.[17] The reaction mixture was heated at a constant rate of 3 °C min^{-1} from room temperature to 370 °C.

In situ pair distribution function analysis experiments were executed using beamline 11-ID-C (λ = 0.11165 Å) at the Advanced Photon Source at Argonne National Laboratory. The reaction mixture was ground in air and packed into a 0.70 mm diameter extruded silica capillary and sealed under vacuum. To heat the reaction mixture, a resistive heater and thermocouple were used as previously described.[17] Diffraction measurements were continuously collected using a 2048 × 2048 pixel PerkinElmer 2D plate detector in 30 s increments, each pattern consisting of three 10 s subframes, while the sample was continuously rotated by 5° along its long axis. For pair distribution function (PDF) experiments, the reaction mixture was heated to the specified temperature at 5 °C min^{-1} and allowed to dwell for 5 min at each temperature before data were collected. The 2D diffraction patterns were then radially integrated using GSAS-II (diffraction) or Fit2D (PDF).[18−21] The pair distribution functions, $G(r)$, were extracted using PDFgetX3[22] and fit using PDFGUI.[23]

Rietveld refinements were executed sequentially in the EXPGUI frontend to GSAS. The full set of diffraction patterns were split into six separate sets based on visual inspection to determine at which temperatures require addition or deletion of phases in the refinement (temperature ranges 28−92 °C, 92−123 °C, 123−163 °C, 163−240 °C, 240−247 °C, 247−283 °C, and 283−367 °C). The lowest temperature in each set was refined by hand and served as a starting point for each sequential refinement. Maximum dampening was applied to all parameters to maintain reasonable values. The fits were then compared within each set, and to the adjacent sets, to confirm adequate fits and continuity across the entire set of diffraction patterns. Phase fractions were extracted from weight percent values and converted to molar percents.

Magnetic measurments were performed using a Quantum Designs Inc. MPMS. Heat capacity measurements were performed using a Quantum Designs Inc. Dynacool PPMS. Differential scanning calorimetry (DSC) measurements were performed using a TA Instruments DSC on samples hermetically sealed in an argon environment. The heating rate for the DSC measurements was 1 °C min^{-1}.

Density functional theory (DFT) calculations with projector-augmented-wave (PAW) potentials with Cu 3p semicore states treated as valence states[24] were implemented using the Vienna Ab Initio Simulation Package (VASP)[25] within the generalized gradient approximation to account for exchange and correlation effects (PBEsol).[26] Ferromagnetic, antiferromagnetic, and nonmagnetic configurations were tested; the nonmagnetic state was lowest in energy. The plane-wave energy cutoff was 800 eV for all calculations, which were performed on a 10 × 10 × 10 and 12 × 10 × 14 k-mesh for pyrite and marcasite, respectively. For ionic relaxations, forces were converged to within 0.01 eV $Å^{-1}$; within each self-consistency cycle, the total energy was converged below 10^{-6} eV. Convergence tests were performed with respect to the Γ-centered k-mesh and band cutoff.

RESULTS

From our DFT calculations, shown in Figure 1c, we confirm that marcasite is 3.0 meV lower in energy in the ground state (electronically for T = 0 K). Furthermore, the calculated energies were fit to a Birch−Murnaghan equation-of-state to extract the ground-state volume and bulk modulus.[15] For marcasite $CuSe_2$, the bulk modulus is B = 78.9 GPa and ground-state volume is V_o = 56.6 $Å^3$ $cell^{-1}$ formula $unit^{-1}$. Pyrite $CuSe_2$ becomes lower in energy at a volume of ∼55.7 $Å^3$ $cell^{-1}$ formula $unit^{-1}$. For marcasite, this would correspond to bulk, volumetric strain of 1.6%, and thus a hydrostatic pressure of ∼1.25 GPa, consistent with the experimental pressures

DOI: 10.1021/ja512520z
J. Am. Chem. Soc. 2015, 137, 3827−3833

reported for bulk synthesis.[3] Despite these differences, the two polymorphs are close in energy.

The metathesis reaction of Na_2Se_2 and $CuCl_2$ was performed in two distinct ways to influence polymorph selection of $CuSe_2$:

$$Na_2Se_2(s) + CuCl_2(s) \xrightarrow[\text{grinding}]{H_2O(g)} \xrightarrow{\Delta} \text{pyrite } CuSe_2(s) + 2NaCl(s) \quad (1)$$

or,

$$Na_2Se_2(s) + CuCl_2(s) \xrightarrow{\Delta} \text{marcasite } CuSe_2(s) + 2NaCl(s) \quad (2)$$

When the reactants are ground in humid air (eq 1), a color change quickly occurs from brown to black, yielding NaCl, Se, and poorly crystallized phases (Figure 2a, bottom). The

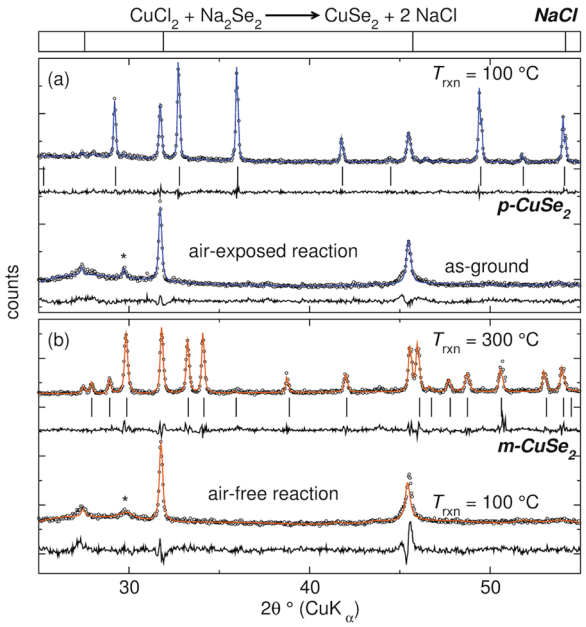

Figure 2. PXRD (black symbols) comparison of metathesis products from reactions that have been (a) air-exposed and (b) strictly air-free, along with their Rietveld analyses (colored lines) and difference curves (black lines). Asterisks indicate reflections from crystalline Se. The expected reflections of NaCl are shown above the refinements.

mixture does not deliquesce. Annealing this mixture at 100 °C (for 24 h) *in vacuo* quantitatively yields bulk pyrite $CuSe_2$ (Figure 2a, top). While water inclusion into the crystal structure of pyrite $CuSe_2$ cannot be shown unequivocally, the data suggest that defects in the crystal structure are minimal. The lattice parameter extracted from the Rietveld refinement of the washed pyrite $CuSe_2$ product is 6.125(1) Å, which is 0.2% larger than the reported 6.116(1) Å.[3] Reaction of air-exposed $CuCl_2$ + Na_2Se_2 at 100 °C for 6 weeks yielded a mixture of both marcasite and pyrite $CuSe_2$, suggesting that the water does not provide a thermodynamic preference for the pyrite polymorph.

The physical properties of pyrite $CuSe_2$ produced under kinetic control were measured to confirm formation of a pure product that exhibits bulk superconductivity. Temperature-dependent magnetic susceptibility measurements reveal a significant diamagnetic response indicative of bulk superconductivity below T_c = 2.4 K, with bulk volume exclusion of the magnetic field ($4\pi\chi \sim -1$ emu cm^{-3}) (Figure 3a). The

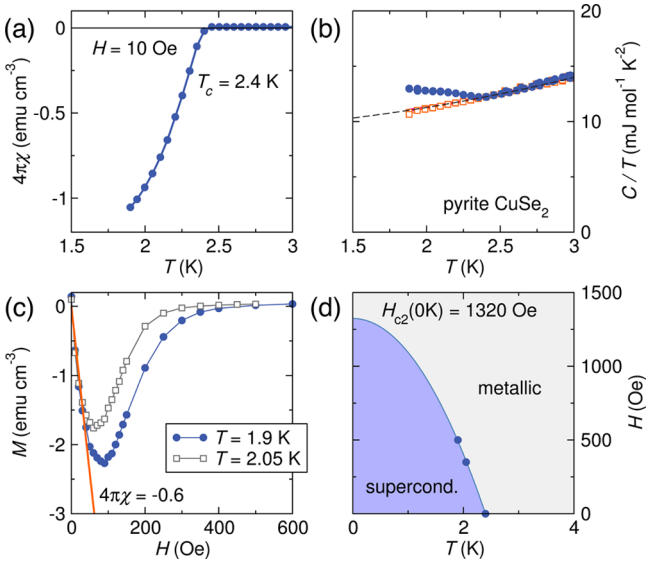

Figure 3. Physical properties of the washed pyrite $CuSe_2$ prepared under kinetic control. (a) Magnetic susceptibility as a function of temperature in a 10 Oe field yields a diamagnetic transition at 2.4 K. (b) Heat capacity divided by temperature as a function of temperature in a 10 Oe field (blue) and 1000 Oe field (orange) shows an increase in heat capacity at the same temperature, indicative of a superconducting transition. (c) Magnetic susceptibility as a function of field at multiple temperatures allows the formation of (d) an electronic phase diagram. The line between the two phases traces $H_{c2}(T)$.

superconducting transition temperature is unaffected, and H_{c2} is small; together, these suggest that there are no significant inclusions into the crystal structure.[27,28] The magnetic susceptibility below T_c indicates total exclusion of magnetic flux from the material and bulk superconductivity, which would not be the case with extensive H_2O inclusion into the crystal structure. Heat capacity measurements also indicate superconductivity, showing the beginning of the jump in the specific heat below T_c. The lack of a sharp jump likely indicates the presence of defects within the crystal, as expected from the low-temperature preparatory route (Figure 3b), but is also observed in many other materials (e.g., $Fe_{1+\delta}Se$).[29] Application of a moderately low magnetic field removes the anomaly in the specific heat, as expected given the low H_{c2} of the superconducting state.

Measurements of magnetization as a function of applied field at varied temperatures of the bulk superconductor pyrite $CuSe_2$ indicate that pyrite is a type-II superconductor. Using a two-fluid model ($H_{c2}[T] = H_{c2}[0\text{ K}][1 - (T/T_c)^2]$), we estimate $H_{c2}[0\text{ K}] \sim 1320$ Oe (Figure 3c). From this, an electronic phase diagram can be constructed describing the superconducting behavior of the material as a function of temperature and applied field (Figure 3d), thus confirming the bulk properties of the material.

When reacted under strictly anhydrous conditions (eq 2), no product is formed at T_{rxn} = 100 °C after 24 h. NaCl only crystallizes upon exposure to the atmosphere when preparing the sample for powder X-ray diffraction (PXRD) (Figure 2b, bottom). This was also confirmed by air-free diffraction of the product in a sealed glass capillary, which showed only starting materials. As a control, incubation of the anhydrous mixture in dry O_2(g) for 24 h before annealing does not promote a reaction, which suggests that humidity plays a role. When

DOI: 10.1021/ja512520z
J. Am. Chem. Soc. 2015, 137, 3827−3833

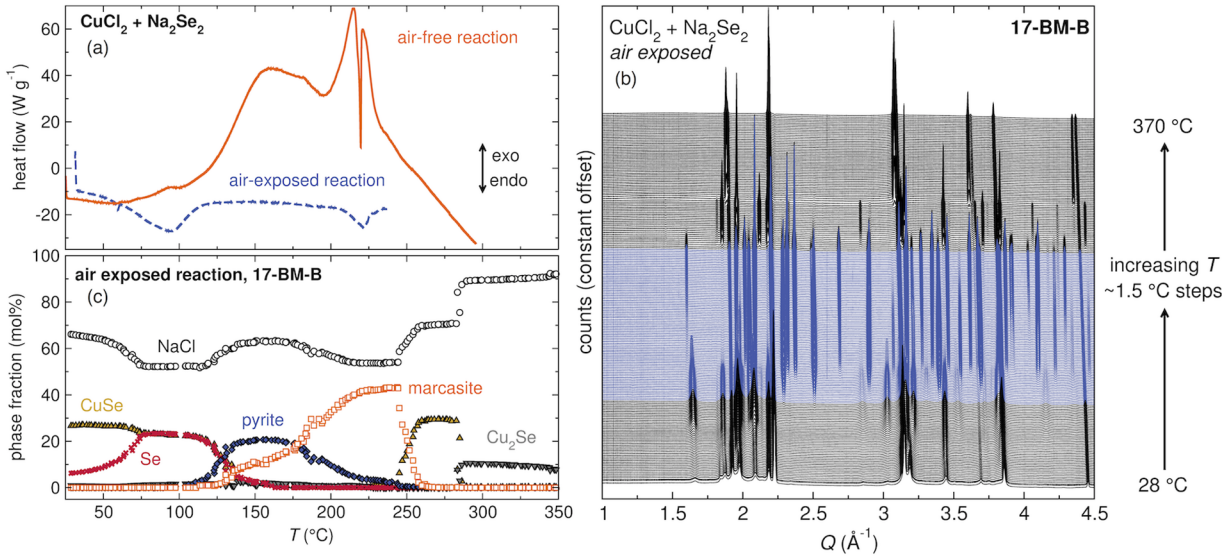

Figure 4. (a) DSC curves of the air-free (orange) and air-exposed (blue) reaction of $CuCl_2$ and Na_2Se_2. (b) *In situ* SXRD data collected from the air-exposed reaction mixture, as heated under vacuum. (c) The extracted phase fractions from the Rietveld refinements of the *in situ* SXRD measurements of the air-exposed reaction.

annealed at 300 °C without exposure to the atmosphere, marcasite $CuSe_2$ forms (Figure 2b, top, eq 2).

The reaction pathway was probed with both *in situ* synchrotron X-ray diffraction (SXRD) and DSC in order to understand the nature of intermediate products (Figure 4). The energetics of the reaction vary drastically with alteration of the preparatory route. When ground in air, no exotherms are detected by DSC, but rather a small endotherm near T = 100 °C coincides with the initial formation of pyrite $CuSe_2$ (Figure 4a). The air-free sample shows significant exotherms as the reaction is heated and NaCl forms (since there is none present after heating at T = 100 °C). Both samples show an endotherm around T = 220 °C, likely due to the melting of selenium.

In situ SXRD of the reaction that produces pyrite $CuSe_2$ elucidates the nature of intermediates and decomposition products (Figure 4b). After grinding in air and before heating, NaCl, CuSe, and Se are observed as well as a trace amount of Cu_2Se. As the reaction mixture is heated, the crystalline intermediates (Covellite CuSe and Se) react to form pyrite, followed by marcasite at slightly higher temperatures.

Quantitative phase analysis of the diffraction data with the Rietveld method show that NaCl formation is quantitative before heating. The relative phase fraction only changes due to the increase or decrease of other crystalline components in the reaction mixture (Figure 4c). As the reaction mixture is heated, the selenium further crystallizes, noted by a sharpening of Bragg peaks and the decrease in background, which is consistent with the presence of a noncrystalline Se component in the as-ground mixture (Figure S1). By $T \sim 75$ °C, CuSe and Se formation is quantitative with 2 NaCl. From this mixture, pyrite begins to form at $T \sim 90$ °C, at the expense of CuSe and Se, as per the reaction CuSe + Se → p-$CuSe_2$. The onset of marcasite formation occurs at ~110 °C, along with continued pyrite growth. The phase fraction of pyrite begins to decline at $T \sim 175$ °C as the phase fraction of marcasite increases. As the temperature continues to increase, a two-step decomposition occurs to CuSe and Cu_2Se at $T \sim 245$ °C and 280 °C, respectively.

PDF analysis of the total scattering data reveals minimal changes to the local atomic separations for low reaction temperatures, despite the myriad transformations between crystalline phases (Figure 5). While the overlap of multiple phases precludes a unique description of $G(r)$, at temperatures below T = 140 °C, the local structure is consistent with a linear combination of CuSe [28(11) mol %], pyrite [11(8) mol %], and NaCl [61(17) mol %]. Above T = 140 °C, removal of CuSe provides a better description of the PDFs [$CuSe_2$: 36(7) mol %; NaCl: 64(7) mol %, Figure 5]. Additionally at low temperatures, the nearest-neighbor correlation is not well described, which suggests there there are poorly ordered phases between the crystalline phases. While the *in situ* PXRD shows a vast number of changes at low temperatures, the local structure does not, which suggests that there are close structural

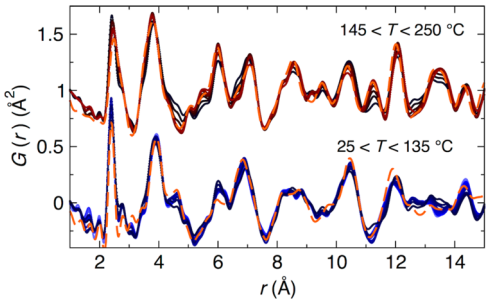

Figure 5. PDF analysis of the synchrotron PXRD data. No major changes in the local structure occur below 145 °C, which suggests that the intermediate structures have close relationships to one another. At these lower temperatures, the phases NaCl, CuSe, pyrite $CuSe_2$ provide a reasonable description of the local structure, whereas NaCl, marcasite, pyrite, and CuSe are found at the higher temperatures. At the shortest distances (r = 2.2–2.3), there is some intensity in $G(r)$ that is not accounted for by the calculated patterns, which suggests the presence of some poorly ordered or amorphous components (fit curve: dashed orange lines; higher temperature data offset for clarity).

DOI: 10.1021/ja512520z
J. Am. Chem. Soc. 2015, 137, 3827–3833

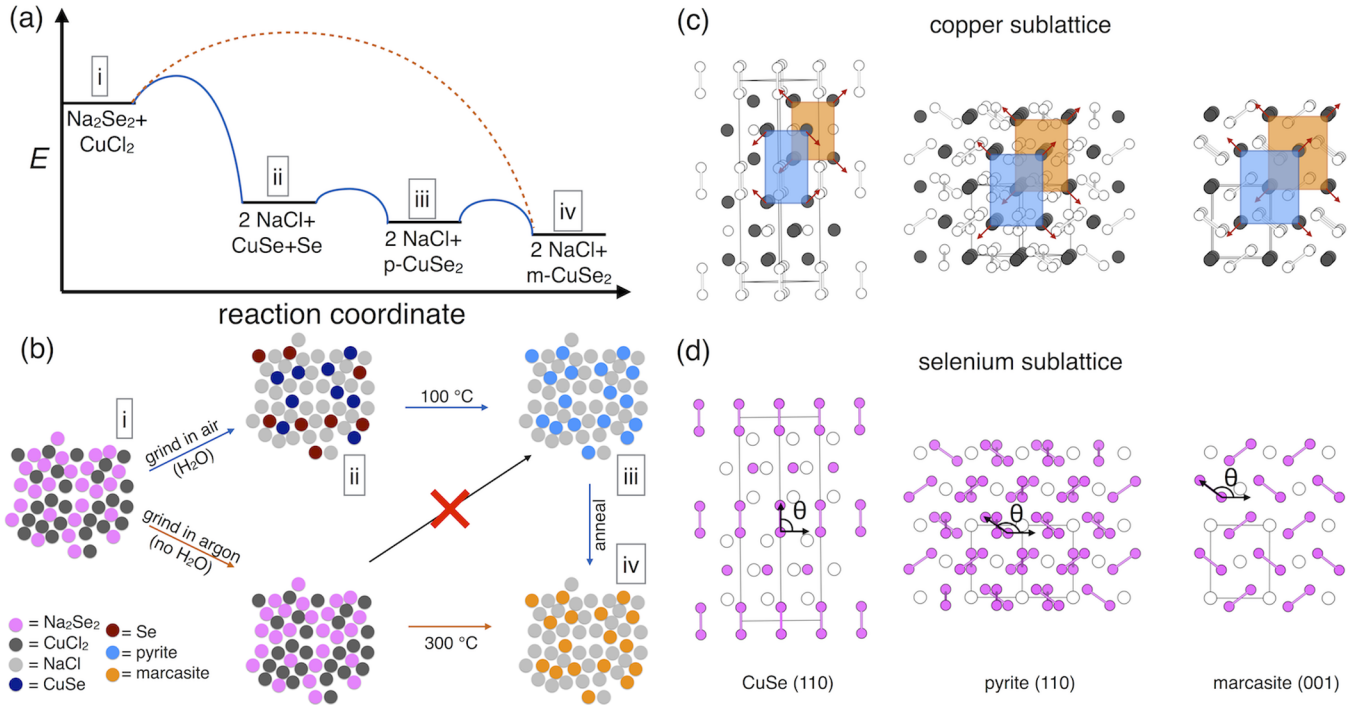

Figure 6. (a) Proposed schematic reaction pathway that permits kinetic control of pyrite $CuSe_2$ formation through air exposure. Grinding in air dissipates a large amount of energy through NaCl formation, minimizing the enthalpy difference between the intermediates and pyrite $CuSe_2$ phase. (b) A simplified, proposed reaction scheme of the selective formation of either pyrite or marcasite $CuSe_2$ through solid-state metathesis. The key difference between the formation pathways is that air exposure, and thus partial solvation, is necessary to form the reaction intermediates that transform into pyrite. Without partial solvation, pyrite $CuSe_2$ formation is not possible through metathesis. The Roman numerals correspond to the different energy levels in (a). Comparison of the (c) copper and (d) selenium sublattices in covellite CuSe, pyrite $CuSe_2$, and marcasite $CuSe_2$. The transition between the three structures can be explained by a progression of expansion and relaxation. Counterions are shown in white. The corresponding changes in the Cu−Cu distances and selenium dimer rotation are listed in Table 1.

relationships between the intermediates (CuSe and Se) and product, pyrite $CuSe_2$.

DISCUSSION

While solid-state metathesis has been extensively explored as a rapid synthetic approach to the formation of refractory borides, carbides, silicides, pnictides, and chalcogenides, these reactions often proceed violently through a propagating ignition wave.[30,31] Depending on the precursors used, solid-state metathesis reactions can also be non-self-igniting,[32] and the reactions have recently been shown to take place via metastable crystalline intermediates.[33] Here, the results indicate that the reaction proceeds at low temperature, thus allowing for kinetic control. This refers to the isolation of the metastable pyrite $CuSe_2$ polymorph, which would be otherwise impossible if executed at higher temperatures, where only marcasite $CuSe_2$ forms. The distinct reactivity between the air-free and air-exposed reactions originates from partial solvation of the reaction mixture. Liquid-assisted mechanochemical reactions have also been used to alter reactions that form organic molecules and metal−organic frameworks,[34,35] and surface hydration has been shown to control polymorphism of nanocrystalline ZnS.[36] Here, partial hydration appears to influence the activation barriers separating crystalline intermediates.

Based on our experimental observations, the schematic reaction coordinate diagram proposed in Figure 6a illustrates how kinetic control is likely accomplished. When ground in air, no exotherms appear in the DSC data, because NaCl has already been formed upon grinding, as confirmed by PXRD (Figures 2a and 4b). We infer that partial hydration of the reactants increases the mobility of the sodium and chloride ions in the solid matrix, which react to form NaCl with a low activation barrier. This in turn drives forward the formation of CuSe and crystalline selenium through the displacement of the remaining ions. Concomitantly, the small endotherm between 60 and 100 °C in the air-exposed reaction, indicates that (a) the energy from forming NaCl has already been released and (b) a small activation barrier must be overcome for CuSe and Se to react to form pyrite $CuSe_2$. Upon further heating ($T \sim 130$ °C), the third activation barrier is overcome as pyrite recrystallizes into marcasite $CuSe_2$.

These results are summarized in Figure 6b, the steps of which are correlated to the reaction coordinate in Figure 6a. Grinding the reactants in air allows energy to be dissipated through the formation of NaCl without exogenous heating (i → ii). From the intermediates of CuSe and Se, heating forms pyrite, then marcasite (ii → iii → iv). Without the initial exposure to air, more heat must be applied to the system, in order to (a) overcome a larger activation barrier which (b) releases sufficient energy from NaCl formation as to drive formation of the most-stable product, marcasite $CuSe_2$ (i → iv).

As a control, CuSe (prepared from the elements) and Se were reacted at T_{rxn}= 100 °C. After 24 h, a small amount of pyrite was detected in the products as well as unreacted CuSe and selenium. After heating the same reaction mixture for 72 h, there are equal amounts of pyrite and marcasite as well as reactants. After 8 weeks, four times as much marcasite as pyrite is detected as well as a small amount of CuSe + Se. As another control, marcasite $CuSe_2$ was mixed with 2 equiv of NaCl and

DOI: 10.1021/ja512520z
J. Am. Chem. Soc. 2015, 137, 3827−3833

held at T = 100 °C for 500 h; no pyrite $CuSe_2$ is detected in the products. These controls demonstrate that pyrite $CuSe_2$ is a kinetic product and is in fact metastable at T = 100 °C. Previously, mechanochemical reaction of the elements by ball-milling has yielded a mixture of pyrite and marcasite $CuSe_2$, but no phase selectivity or purity was shown.[37]

An additional control of air-exposed $CuCl_2$ + Na_2Se_2 was reacted at 100 °C for 6 weeks. After this long reaction time, both marcasite and pyrite $CuSe_2$ were detected, providing further confirmation of the metastability of the pyrite polymorph. To determine that it was indeed atmospheric H_2O that caused the transition from $CuCl_2$ + Na_2Se_2 → 2NaCl + CuSe + Se, a silica tube containing the reactants was sealed with 1/3 of an atmosphere of O_2, and no reaction or color change was observed after heating to 100 °C for 24 h. Additionally, exposure to N_2 shows no alteration in the reaction mixture.

The activation barriers separating each intermediate phase must be sufficiently small, as the transformations occur at relatively low temperatures. While cursory inspection of the different crystal structures of CuSe, Se, and pyrite $CuSe_2$ reveals many differences (e.g., distinct Cu coordination, different symmetries and connectivities[3,38]), the lack of significant changes in the PDFs as CuSe and Se transform into pyrite below 140 °C (Figure 5) suggests a close structural relationship between these phases. After closer inspection of the reported crystal structures, it is possible to map a displacive transformation with intercalation between the phases.

To illustrate the relationship, the copper and selenium sublattices are compared separately (Figure 6c,d, respectively). Projection of the copper sublattices comprises overlapping rectangles in the {100}, {101}, and {001} lattice planes for covellite CuSe, pyrite $CuSe_2$, and marcasite $CuSe_2$, respectively (Figure 6c). Alternative crystallographic orientations are depicted in Figure S2. The transformations between the phases can be expressed as expansions and relaxations of rectangles connecting Cu atoms. In CuSe, there are two different sizes of rectangles (Table 1). As selenium reacts with the CuSe lattice, the larger rectangles shorten and widen, while the smaller rectangles widen and lengthen. This follows with formation of Se−Se dimers in the trigonal planar Cu−Se {004} layers, which fall in the center of the of the smaller rectangles. Additionally, the space between the rectangles increases as selenium intercalates.

Table 1. Parameters of the Phase Transitions Between CuSe, Pyrite, And Marcasite, as Shown in Figure 6c,d

	copper sublattice parameters[a]		
	CuSe	pyrite	marcasite
a'	4.93, 6.15	6.12	6.18
b'	3.94	4.32	5.01
plane spacing (Å)	1.97	2.16	2.50
	selenium sublattice parameters[a]		
	CuSe	pyrite	marcasite
θ	90	125	143
dimer−dimer (Å)	3.94	4.32	5.01
layer−layer (Å)	4.31	3.06	3.09
Se−Se (Å)	2.28	2.35	2.33

[a]Determined from the reported crystal structures of CuSe,[38] p-$CuSe_2$,[39] and m-$CuSe_2$[39] using VESTA.[40]

The selenium sublattice of CuSe is comprised of both $[Se_2]^{2-}$ dimers (shown with bonds in Figure 6d) and discrete Se^{2-} anions.[41,42] As additional selenium intercalates into the layers of Se^{2-} anions to form dimers, the pre-existing dimers tilt away from the c-axis of CuSe. The pyrite $CuSe_2$ selenium sublattice consists of these Se dimers, tilted either along the plane (as shown) or rotated by 90 deg. As they tilt, the distance between nearest-neighbor dimers increases compared to CuSe, but the layers become close-packed and the Se−Se bond length increases ($CuSe_2$ can be described as two interpenetrating face-centered cubic (fcc) lattices, with one fcc lattice of copper, and the other formed by the center-of-mass of the dimer).[5]

To convert pyrite to marcasite, both the copper and selenium sublattices further relax. The rectangular planes of copper atoms increase in size and move further from one another. The Se−Se dimers relax further off-axis and reorient along the same direction, thus losing the close-packed nature of the pyrite structure.

CONCLUSION

While many metastable phases can be formed by tuning an extrinsic thermodynamic parameter (e.g., temperature, pressure, dielectric constant of a solvent), quantitative isolation of the metastable, high-pressure superconducting polymorph of $CuSe_2$ was achieved via kinetic control of solid-state metathesis. The titration of the enthalpy release from NaCl formation enables the reaction to proceed through kinetic control. From close analysis of the reaction pathway using *in situ* X-ray scattering, the activation barriers are limited by displacive structural rearrangement of crystalline intermediates (CuSe and Se): pyrite $CuSe_2$ is a kinetic intermediate in the reaction CuSe + Se → marcasite $CuSe_2$: intercalation of selenium into the CuSe lattice forces the structure to form pyrite on its way to marcasite. Heating the reaction for longer times or higher temperatures leads to recrystallization into the equilibrium marcasite $CuSe_2$ polymorph. This reaction can be thought of as a manifestation of the Ostwald step rule,[43] whereby less stable intermediates form first, since formation of their surface is less energetically costly than the most stable polymorph.[44] These findings provide broad implications for achieving materials by design and the discovery of new, functional materials, demonstrating how altering chemical pathways can influence the crystal structure and thus the properties of the material.

ASSOCIATED CONTENT

Supporting Information

The supporting information includes two figures that illustrate (a) in situ x-ray diffraction data showing the crystallization of Se as temperature increases, and (b) a different orientation of the proposed structural rearrangement. This material is available free of charge via the Internet at http://pubs.acs.org.

AUTHOR INFORMATION

Corresponding Author

*james.neilson@colostate.edu

Notes

The authors declare no competing financial interest.

ACKNOWLEDGMENTS

The research reported was supported in part by the Energy Institute at Colorado State University. This research used resources of the Advanced Photon Source, a U.S. Department

DOI: 10.1021/ja512520z
J. Am. Chem. Soc. 2015, 137, 3827−3833

of Energy (DOE) Office of Science User Facility operated for the DOE Office of Science by Argonne National Laboratory under contract no. DE-AC02-06CH11357. This research utilized the CSU ISTeC Cray HPC System supported by NSF Grant CNS-0923386. The authors acknowledge Dr. G. Halder (17-BM-B) and Dr. O. Borkiewicz (11-ID-C) of the Advanced Photon Source for assistance with *in situ* XRD and PDF data collection.

REFERENCES

(1) Sharma, K.; Chang, Y. *J. Phase Equilib.* **1996**, *17*, 261−266.
(2) Ranade, M. R.; Navrotsky, A.; Zhang, H. Z.; Banfield, J. F.; Elder, S. H.; Zaban, A.; Borse, P. H.; Kulkarni, S. K.; Doran, G. S.; Whitfield, H. J. *Proc. Natl. Acad. Sci. U.S.A.* **2002**, *99*, 6476−6481.
(3) Bither, T. A.; Bouchard, R. J.; Cloud, W. H.; Donohue, P. C.; Siemons, W. J. *Inorg. Chem.* **1968**, *7*, 2208−2220.
(4) Qi, Y.; Matsuishi, S.; Guo, J.; Mizoguchi, H.; Hosono, H. *Phys. Rev. Lett.* **2012**, *109*, 217002.
(5) Tossell, J.; Vaughan, D.; Burdett, J. *Phys. Chem. Miner.* **1981**, *7*, 177−184.
(6) Hull, G. W.; Hulliger, F. *Nature* **1968**, *220*, 257−258.
(7) Schollhorn, R. *Angew. Chem., Int. Ed.* **1988**, *27*, 1392−1400.
(8) Schleich, D. *Solid State Ionics* **1994**, *70/71*, 407−411.
(9) Rouxel, J.; Tournoux, M. *Solid State Ionics* **1996**, *84*, 141−149.
(10) Gopalakrishnan, J.; Bhuvanesh, N. S. P.; Rangan, K. K. *Curr. Opin. Solid State Mater. Sci.* **1996**, *1*, 285−294.
(11) Neilson, J. R.; McQueen, T. M. *J. Am. Chem. Soc.* **2012**, *134*, 7750−7757.
(12) Murphy, D. W.; Cros, C.; Di Salvo, F. J.; Waszczak, J. V. *Inorg. Chem.* **1977**, *16*, 3027−3031.
(13) Kanatzidis, M. G.; Park, Y. *Chem. Mater.* **1990**, *2*, 99−101.
(14) Shoemaker, D. P.; Hu, Y.-J.; Chung, D. Y.; Halder, G. J.; Chupas, P. J.; Soderholm, L.; Mitchell, J. F.; Kanatzidis, M. G. *Proc. Natl. Acad. Sci. U.S.A.* **2014**, *111*, 10922−10927.
(15) Murnaghan, F. D. *Proc. Natl. Acad. Sci. U.S.A.* **1944**, *30*, 244−247.
(16) Cohen, K.; Rivet, J.; Dugué, J. *J. Alloys Compd.* **1995**, *224*, 316−329.
(17) Chupas, P. J.; Chapman, K. W.; Kurtz, C.; Hanson, J. C.; Lee, P. L.; Grey, C. P. *J. Appl. Crystallogr.* **2008**, *41*, 822−824.
(18) Hammersley, A. P.; Svensson, S. O.; Hanfland, M.; Fitch, A. N.; Hausermann, D. *High Pressure Res.* **1996**, *14*, 235−248.
(19) Toby, B. H. *J. Appl. Crystallogr.* **2001**, *34*, 210−213.
(20) Larson, A., Von Dreele, R. *General Structure Analysis System (GSAS)*; Los Alamos National Lab: Los Alamos, NM, 2004.
(21) Toby, B. H.; Von Dreele, R. B. *J. Appl. Crystallogr.* **2013**, *46*, 544−549.
(22) Juhás, P.; Davis, T.; Farrow, C. L.; Billinge, S. J. L. *J. Appl. Crystallogr.* **2013**, *46*, 560−566.
(23) Farrow, C. L.; Juhas, P.; Liu, J. W.; Bryndin, D.; Božin, E. S.; Bloch, J.; Proffen, T.; Billinge, S. J. L. *J. Phys.-Condens. Mater.* **2007**, *19*, 335219.
(24) Kresse, G.; Joubert, D. *Phys. Rev. B* **1999**, *59*, 1758.
(25) Kresse, G.; Furthmüller, J. *Phys. Rev. B* **1996**, *54*, 11169.
(26) Perdew, J. P.; Ruzsinszky, A.; Csonka, G. I.; Vydrov, O. A.; Scuseria, G. E.; Constantin, L. A.; Zhou, X.; Burke, K. *Phys. Rev. Lett.* **2008**, *100*, 136406.
(27) Mao, Z. Q.; Mori, Y.; Maeno, Y. *Phys. Rev. B* **1999**, *60*, 610−614.
(28) Serquis, A.; Zhu, Y. T.; Peterson, E. J.; Coulter, J. Y.; Peterson, D. E.; Mueller, F. M. *Appl. Phys. Lett.* **2001**, *79*, 4399−4401.
(29) McQueen, T. M.; Huang, Q.; Ksenofontov, V.; Felser, C.; Xu, Q.; Zandbergen, H.; Hor, Y. S.; Allred, J.; Williams, A. J.; Qu, D.; Checkelsky, J.; Ong, N. P.; Cava, R. J. *Phys. Rev. B* **2009**, *79*, 014522.
(30) Bonneau, P. R.; Jarvis, R. F.; Kaner, R. B. *Nature* **1991**, *349*, 510−512.
(31) Parkin, I. P. *Chem. Soc. Rev.* **1996**, *25*, 199−207.
(32) Shaw, G. A.; Morrison, D. E.; Parkin, I. P. *J. Chem. Soc., Dalton Trans.* **2001**, 1872−1875.
(33) Martinolich, A. J.; Neilson, J. R. *J. Am. Chem. Soc.* **2014**, *136*, 15654−15659.
(34) Belenguer, A. M.; Lampronti, G. I.; Wales, D. J.; Sanders, J. K. M. *J. Am. Chem. Soc.* **2014**, *136*, 16156−16166.
(35) Friščić, T.; Halasz, I.; Beldon, P. J.; Belenguer, A. M.; Adams, F.; Kimber, S. A. J.; Honkimäki, V.; Dinnebier, R. E. *Nat. Chem.* **2013**, *5*, 66−73.
(36) Zhang, H.; Gilbert, B.; Huang, F.; Banfield, J. F. *Nature* **2003**, *424*, 1025−1029.
(37) Ohtani, T.; Motoki, M.; Koh, K.; Ohshima, K. *Mater. Res. Bull.* **1995**, *30*, 1495−1504.
(38) Berry, L. G. *Am. Mineral.* **1954**, *39*, 504−509.
(39) Heyding, R. D.; Murray, R. M. *Can. J. Chem.* **1976**, *54*, 841−848.
(40) Momma, K.; Izumi, F. *J. Appl. Crystallogr.* **2011**, *44*, 1272−1276.
(41) Kumar, P.; Nagarajan, R.; Sarangi, R. *J. Mater. Chem. C* **2013**, *1*, 2448−2454.
(42) Conejeros, S.; Moreira, I. d. P. R.; Alemany, P.; Canadell, E. *Inorg. Chem.* **2014**, *53*, 12402−12406.
(43) Ostwald, W. *Z. Phys. Chem.* **1897**, *22*, 289−330.
(44) Navrotsky, A. *Proc. Natl. Acad. Sci. U.S.A.* **2004**, *101*, 12096−12101.

DOI: 10.1021/ja512520z
J. Am. Chem. Soc. 2015, 137, 3827−3833